2026 IEEE International Conference on Robotics and Automation (ICRA 2026)
June 1-5, 2026. Vienna, Austria

NDO-Based Dual Quaternion Control of a Drone with a Cable-suspended Load

Yuxia Yuan, Junjie Kang, Jinjun Shan, *Senior Member, IEEE*, Markus Ryll, *Member, IEEE*

***Abstract*— This paper proposes a novel nonlinear disturbance observer (NDO) based dual quaternion dynamics modeling and control framework for a drone with a cable-suspended load. Leveraging dual quaternions, a compact and singularity-free mathematical representation, we derive a unified dynamic model that captures the coupled translational and rotational dynamics of both the drone and the slung load. NDOs are designed to estimate and compensate for uncertainties and external disturbances affecting the drone and the load. Building on this framework, we develop a robust control strategy that ensures precise trajectory tracking of the slung load while maintaining stable drone attitude control. The effectiveness of the proposed approach is validated through comprehensive simulations and real-world experiments on a cargo drone platform. The results highlight the robustness and reliability of the system in practical scenarios, demonstrating its potential application in cargo transportation.**

I. Introduction

Aerial vehicles have become indispensable in a wide range of applications, from aerial surveillance and environmental monitoring to logistics and cargo transportation [1]. Among these, cargo transportation has emerged as a particularly promising domain. Drones equipped with cable-suspended loads offer a practical and efficient solution for transporting large, heavy, or irregularly shaped objects in environments where ground-based transportation is limited or infeasible, such as mountainous terrains, disaster relief zones, and industrial sites [2]. However, drones with cable-suspended loads introduce several critical challenges. The primary issue arises from the dynamic coupling between the drone and the load, resulting in a system with complex, nonlinear, and underactuated properties [3]. The swinging motion of the load can induce oscillations that destabilize the drone, compromise trajectory tracking accuracy, and pose a risk of collisions with nearby structures [4], [5]. Meanwhile, system uncertainties, such as load mass, cable length, and offset between the attachment point and center of mass (CoM) of the drone further exacerbate these issues [6].

These challenges raise several fundamental research questions: How can we develop accurate models that capture the coupled translational and rotational dynamics of both the drone and the suspended load? How can disturbance estimation techniques be integrated into drone control frameworks to enhance resilience against environmental perturbations? What robust control strategies can ensure stability and precise trajectory tracking in the presence of system parameter uncertainties and external disturbances? Addressing these questions is crucial to unlock the full potential of cargo drones with slung loads for real-world deployment.

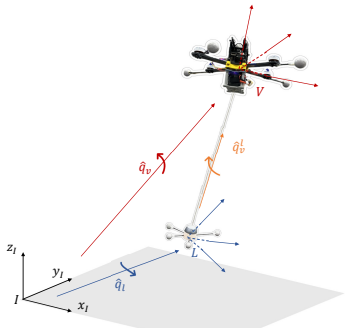

Fig. 1: Dual quaternion transformation among three frames. $\hat{q}_v$ denotes the transformation from the inertial frame I to drone body frame V, and $\hat{q}_l$ is the transformation from I to load body frame L. $\hat{q}_v^l$ indicates the transformation from L to V.

To develop accurate models that capture the coupled translational and rotational dynamics of both a drone and its suspended load, researchers have utilized the Newton-Euler equations and the Lagrangian formulation to derive motion equations that account for the nonlinear interactions between the drone and the suspended load, such as those captured by the geometric model [3]. Unit dual quaternions, a mathematical framework that unifies translational and rotational dynamics into a single representation, have been applied to formulate the dynamic model of cargo drones [7]. Compared with models based on Euler angles or rotation matrix [3], it offers a compact, computationally efficient, and singularity-free way to describe the coupled system dynamics [8].

In order to improve stability and precise trajectory tracking in cargo drone systems with uncertainties and disturbances, various control laws have been extensively studied. Model predictive control (MPC) strategies have been applied to the control of cargo drones with slung-load to achieve a balance between rapid stabilization and minimal load swing [4], [9]. Some improved MPC frameworks can be used to tackle specific research problems, such as by integrating a sliding mode to reject bounded matched perturbations [10], and using a hybrid nonlinear model to address the challenges posed by dual motion modes [11]. Besides, adaptive robust

Yuxia Yuan is with the Autonomous Aerial Systems, School of Engineering and Design, Technical University of Munich, 85521 Ottobrunn, Germany (e-mail: yuxia.yuan@tum.de).

Junjie Kang and Jinjun Shan are with the Department of Earth and Space Science and Engineering, York University, Toronto, ON M3J 1P3, Canada (e-mail: kjj@yorku.ca; jjshan@yorku.ca).

Markus Ryll is with Munich Institute of Robotics and Machine Intelligence (MIRMI) and Autonomous Aerial Systems, School of Engineering and Design, Technical University of Munich, Lise-Meitner-Straße 9, 85521 Ottobrunn, Germany. (e-mail: markus.ryll@tum.de)

control strategies have been employed in cargo drone control to address parametric uncertainties and disturbances [12]. For example, Kang and Shan [13] proposed a smooth coupling-enhanced adaptive controller to address the parameter uncertainties of a drone with a slung load.

However, both MPC and adaptive control require an accurate model of the drone with a slung load system that is highly nonlinear and has coupled dynamics. Moreover, while adaptive control can handle certain parametric uncertainties and MPC can explicitly account for constraints and prediction horizons, neither method alone guarantees robust performance under significant external disturbances or rapidly changing operating conditions. Nonlinear disturbance observers (NDOs) have emerged as a robust tool to improve control performance in the presence of uncertainties and disturbances [14]. Recent studies have demonstrated the effectiveness of NDOs in drone systems, showing improved trajectory tracking and disturbance rejection capabilities [15].

Building on a previous work [7], this paper proposes a novel NDO-based control strategy to enhance the stability and accuracy of cargo drone operations. Our key contributions are as follows. First, we introduce a hybrid dynamic model for a cargo drone system that accounts for both slack and taut cable conditions, extending the dual quaternion dynamic model presented in [7]. By leveraging the unit dual quaternion framework, the coupled translational and rotational dynamics of the drone–load system are represented within a unified algebraic structure, enabling a homogeneous treatment of pose and twist across subsystems. This enhancement provides a compact and consistent representation of the load dynamics under hybrid conditions. Next, nonlinear disturbance observers (NDOs) are designed to estimate and compensate for system uncertainties and external disturbances. The observers are integrated directly into the dual quaternion pose–twist dynamics, leading to a structurally coherent control formulation. Finally, the effectiveness of the proposed hybrid dynamics and dual quaternion control framework is validated through simulations and experimental studies, demonstrating accurate trajectory tracking and robust disturbance rejection under various operating conditions.

The cargo drone system configuration is illustrated in Fig. 1. It also depicts the transformations between the inertial frame, drone body frame, and slung-load frame using dual quaternions. The proposed approach is validated through simulations and experiments on a real cargo drone, demonstrating improved performance compared to traditional geometric controllers. This work not only tackles key technical challenges in cargo drone control but also paves the way for deploying cargo drones in complex operational scenarios.

II. Notation and Preliminary Knowledge

A. Notations

In the following, subscripts v, l, c denote the drone (aerial **v**ehicle), the **l**oad, and the **c**able, respectively. Superscript r represents the reference states. Superscript V indicates the drone body frame, and we omit the superscript when a variable is expressed in the inertial frame I. The operator $\boldsymbol{a}_\times \boldsymbol{b}$ denotes the cross product $\boldsymbol{a} \times \boldsymbol{b}$, and $\boldsymbol{a}^T \boldsymbol{b}$ represents the dot product $\boldsymbol{a} \cdot \boldsymbol{b}$. The symbols $\bar{q}, \hat{q} \in \mathbb{H}$ denote a quaternion and a dual quaternion, respectively, while $\boldsymbol{v} \in \mathbb{R}^4$ and $\hat{\boldsymbol{v}} \in \mathbb{H}$ indicate a vector quaternion and a dual vector quaternion. Notations $\bar{I}, \bar{0} \in \mathbb{H}$ indicate the identity quaternion and the zero quaternion.

B. Dual Quaternion Operations

The cargo drone, consisting of a drone and a slung load, can be modeled as two coupled subsystems, which involves three reference frames [3], [7], as shown in Fig. 1. The transformation between frames is represented using dual quaternions [16]. A dual quaternion, denoted as $\hat{q} = \bar{q}_r + \bar{q}_d\epsilon$, comprises two quaternions $\bar{q}_r, \bar{q}_d \in \mathbb{H}$. The real part $\bar{q}_r$ is a unit quaternion representing rotation, and the dual part $\bar{q}_d$ encodes translation. The involved operations for dual quaternions are listed below:

- Difference: $\hat{q}_{ab} = \hat{q}_b^* \otimes \hat{q}_a$
- Product: $\hat{q}_1 \otimes \hat{q}_2 = \bar{q}_{1r} \otimes \bar{q}_{2r} + [\bar{q}_{1r} \otimes \bar{q}_{2d} + \bar{q}_{1d} \otimes \bar{q}_{2r}]\epsilon$
- Conjugate: $\hat{q}^* = \bar{q}_r^* + \bar{q}_d^*\epsilon$
- Norm for unit dual quaternions: $||\hat{q}||^2 = 1 + 0\epsilon$
- Inverse for unit dual quaternions: $\hat{q}^{-1} = \hat{q}^*$
- Natural logarithm mapping: $\ln \hat{q} = \frac{1}{2}(\overline{\theta} + T\epsilon)$; $\overline{\theta}$ is the rotation angle vector
- Adjoint transformation: $Ad_{\hat{q}}\hat{r} = \hat{q} \otimes \hat{r} \otimes \hat{q}^*$

A dual vector quaternion is defined as $\hat{\boldsymbol{v}} = \boldsymbol{v}_r + \boldsymbol{v}_d\epsilon$, which is a special case of a dual quaternion in which the scalar components are zero. Specifically, $\hat{\boldsymbol{v}}$ can be equivalently written as a dual quaternion in the form $\hat{\boldsymbol{v}} = [0, \boldsymbol{v}_r] + [0, \boldsymbol{v}_d]\epsilon$. This also implies that any standard vector (or vector quaternion) can be treated as $\boldsymbol{v} = [0, \boldsymbol{v}] \in \mathbb{H}$. In this work, we utilize the dual vector quaternion representation to describe the state of the suspended load.

III. Hybrid Dynamic Model of the Cargo Drone with Slung Load

For a cargo drone with a cable-suspended load system, as illustrated in Fig. 2, the transportation mission can be divided into several stages, as shown in Fig. 3. The cable is slack during the *Setup* and *Landing* phases and may also become slack during other stages if external disturbances, such as wind gusts, occur. Therefore, it is necessary to develop a hybrid model that captures the full system dynamics, rather than assuming that the cable is always taut or always slack [3].

Cable elasticity can be neglected by selecting appropriate materials, which allows us to assume the cable maintains a constant length throughout the mission. Additionally, we assume that transitions between taut and slack conditions occur over a very short timescale. This enables a simplified binary representation of the cable condition: either fully taut or slack. We introduce an indicator σ and $s = 1 - \sigma$ to represent the cable condition during transportation as

$$\sigma = \begin{cases} 1 & \text{otherwise} \\ 0 & ||\boldsymbol{p}_v - \boldsymbol{p}_l|| < l - \delta, \end{cases} \tag{1}$$

where δ is a small positive constant. Treating the drone as a rigid body, we use dual quaternions to represent the dynamics

of a drone [8] in terms of orientation, position, and twist as

$$\hat{q}_v = \bar{q}_v + \frac{1}{2}\boldsymbol{p}_v \otimes \bar{q}_v \epsilon \tag{2}$$

$$\hat{\xi}_v^V = \boldsymbol{\omega}_v^V + [\boldsymbol{\omega}_{v\times}^V \boldsymbol{p}_v + \dot{\boldsymbol{p}}_v^V]\epsilon. \tag{3}$$

$\hat{q}_v$ is the transformation, consisting of the rotational quaternion $\bar{q}_v$ and the translational quaternion $\frac{1}{2}\boldsymbol{p}_v \otimes \bar{q}_v$. $\hat{\xi}_v^V$ is the twist of the body, which combines the rotational velocity $\boldsymbol{\omega}_v^V$ and the translational velocity $\dot{\boldsymbol{p}}_v^V$ and is described in frame V. According to the Newton-Euler approach [17], we get the dynamics as

$$\dot{\hat{q}}_v = \frac{1}{2}\hat{q}_v \otimes \hat{\xi}_v^V \tag{4}$$

$$\dot{\hat{\xi}}_v^V = \dot{\boldsymbol{\omega}}_v^V + [\dot{\boldsymbol{\omega}}_{v\times}^V \boldsymbol{p}_v + \boldsymbol{\omega}_{v\times}^V \dot{\boldsymbol{p}}_v + \ddot{\boldsymbol{p}}_v^V]\epsilon \tag{5}$$

with

$$\dot{\boldsymbol{\omega}}_v^V = \mathbf{J}_v^{-1}(\boldsymbol{\tau}_u - \boldsymbol{\omega}_{v\times}^V \mathbf{J}_v \boldsymbol{\omega}_v^V) + \mathbf{J}_v^{-1}\boldsymbol{d}_v, \tag{6}$$

$$\ddot{\boldsymbol{p}}_v^V = (\boldsymbol{F}_u^V - \sigma \boldsymbol{F}_t^V)/m_v - \boldsymbol{g}_3^V. \tag{7}$$

where $\mathbf{J}_v \in \mathbb{R}^{3\times3}$ is the inertia matrix of the body, and $\boldsymbol{g}_3 = g\boldsymbol{e}_3$ indicates the gravity acceleration. $\boldsymbol{\tau}_u$, $\boldsymbol{F}_u \in \mathbb{R}^3$ are the control inputs. $\boldsymbol{d}_v \in \mathbb{R}^3$ is a disturbance, and $\dot{\boldsymbol{\omega}}_v^V$ is drone's body rate. Due to the coupled dynamics between the drone and its slung load, we define the force vector from the slung-load subsystem via the cable as $\boldsymbol{F}_t = -f_c \boldsymbol{q}_c$, where f_c denotes the tension magnitude in the cable and $\boldsymbol{q}_c$ is the unit vector along the cable pointing from the drone to the load. We then utilize the cable indicator σ to describe the drone's translational dynamics as (7). $\ddot{\boldsymbol{p}}_v^V$ is the linear acceleration of the drone. Together with $\boldsymbol{g}_3^V$, $\boldsymbol{F}_t^V$, and $\boldsymbol{F}_u^V$, they are presented in the body frame V. The transformation from body frame to inertial frame can be obtained by the quaternion product.

$$\boldsymbol{F}_u = \bar{q}_v \otimes \boldsymbol{F}_u^V \otimes \bar{q}_v^*. \tag{8}$$

For the slung-load subsystem, when the cable is slack, there is no tension in the cable, and we have $s = 1$. The load is static on the ground or in free fall under gravity. When the cable is taut with $\sigma = 1$, the load motion is governed by the tension in the cable and gravity, and the holonomic constraints between the drone and the load are satisfied.

$$\boldsymbol{p}_v = \boldsymbol{p}_l - l\boldsymbol{q}_c, \quad \dot{\boldsymbol{p}}_v = \dot{\boldsymbol{p}}_l - l\dot{\boldsymbol{q}}_c \tag{9}$$

By using the Lagrange-d'Alembert principle [3], the motion equations of the slung-load subsystem are derived as

$$m_v l\ddot{\boldsymbol{q}}_c - \boldsymbol{d}_c = \sigma(\boldsymbol{q}_{c\times}(\boldsymbol{q}_{c\times}\boldsymbol{F}_u) - m_v l(\dot{\boldsymbol{q}}_c^T \dot{\boldsymbol{q}}_c)\boldsymbol{q}_c) \tag{10}$$

$$m_l(\ddot{\boldsymbol{p}}_l + \boldsymbol{g}_3) - \boldsymbol{d}_p = \sigma \boldsymbol{F}_t, \tag{11}$$

where $m_{l/v}$ is the mass of the load/drone, l is the length of the cable. $\ddot{\boldsymbol{p}}_l$ and $\ddot{\boldsymbol{q}}_c$ are the linear and angular acceleration of the slung-load subsystem. $\boldsymbol{d}_p$ and $\boldsymbol{d}_c$ introduce disturbances, adding to the load translation and the cable attitude, respectively. By combining (7), (9), and (10), we get $\boldsymbol{F}_t$ as

$$\boldsymbol{F}_t = \frac{m_l(\boldsymbol{q}_c^T \boldsymbol{F}_u \boldsymbol{q}_c - m_v l(\dot{\boldsymbol{q}}_c^T \dot{\boldsymbol{q}}_c)\boldsymbol{q}_c) + m_l \boldsymbol{d}_c - m_v \boldsymbol{d}_p}{m_v + m_l} \tag{12}$$

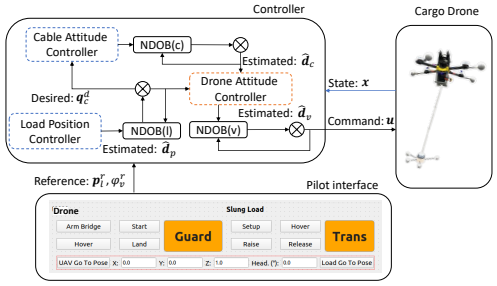

Fig. 2: The diagram of our cargo drone system.

To obtain a compact representation of the hybrid dynamic model for the cargo drone, we use dual vector quaternions to present the dynamics of the slung load. From the definition of dual quaternion (13) and (14), we know the scalar part of every quaternion is zero.

$$\hat{\boldsymbol{q}}_l = \boldsymbol{q}_c + \boldsymbol{p}_l \epsilon \tag{13}$$

$$\hat{\boldsymbol{\xi}}_l = \dot{\boldsymbol{q}}_c + \dot{\boldsymbol{p}}_l \epsilon \tag{14}$$

Combining the dynamic model of the drone, we obtain the dual quaternion dynamic model of the cargo drone with considering the cable condition indicator σ as

$$\dot{x} = \begin{bmatrix} \dot{\hat{\boldsymbol{q}}}_l \\ \dot{\hat{\boldsymbol{\xi}}}_l \\ \dot{\hat{q}}_v \\ \dot{\hat{\xi}}_v^V \end{bmatrix} = \begin{bmatrix} \dot{\boldsymbol{q}}_c + \dot{\boldsymbol{p}}_l \epsilon \\ \hat{F}_l \\ \frac{1}{2}\hat{q}_v \otimes \hat{\xi}_v^V \\ \hat{F}_v \end{bmatrix} + \begin{bmatrix} 0 \\ \hat{u}_l \\ 0 \\ \hat{u}_v \end{bmatrix}, \tag{15}$$

with

$$\hat{u}_l = \sigma(\boldsymbol{q}_{c\times}(\boldsymbol{q}_{c\times}\boldsymbol{F}_u)/(m_v l) + \sigma \boldsymbol{F}_t/(m_l)\epsilon \tag{16}$$

$$\hat{F}_l = -\sigma(\dot{\boldsymbol{q}}_c^T \dot{\boldsymbol{q}}_c)\boldsymbol{q}_c + \boldsymbol{d}_c/(m_v l) + [\boldsymbol{d}_p/(m_l) - \boldsymbol{g}_3]\epsilon \tag{17}$$

$$\hat{u}_v = \mathbf{J}_v^{-1}\boldsymbol{\tau}_u + [\mathbf{J}_v^{-1}\boldsymbol{\tau}_{u\times}\boldsymbol{p}_v + (\boldsymbol{F}_u^V - \sigma \boldsymbol{F}_t^V)/m_v]\epsilon \tag{18}$$

$$\hat{F}_v = \boldsymbol{a}_v + [\boldsymbol{a}_{v\times}\boldsymbol{p}_v + \boldsymbol{\omega}_{v\times}^V \dot{\boldsymbol{p}}_v^V - \boldsymbol{g}_3^V]\epsilon \tag{19}$$

$$\boldsymbol{a}_v = \mathbf{J}_v^{-1}(\boldsymbol{d}_v - \boldsymbol{\omega}_{v\times}^V \mathbf{J}_v \boldsymbol{\omega}_v^V). \tag{20}$$

IV. Control Strategy for Cargo Drone System

In real-world aerial load transportation tasks, model uncertainties and external disturbances can degrade control performance significantly. To enhance the robustness and improve load trajectory tracking performance, we introduce NDOs to estimate and compensate for disturbances in real-time. We adopt a decoupled design where three separate NDOs are developed as shown in Fig. 2: one for the load translational motion, one for cable attitude, and one for the drone rotational dynamics. This modular observer structure simplifies the observer derivation and implementation, while enabling reliable and effective disturbance compensation for each subsystem. These NDOs are then integrated with the proposed control strategy in Sec.IV-B, which achieves a practical balance between theoretical rigor and experimental feasibility.

A. Nonlinear Disturbance Observer (NDO)

Firstly, we design an NDO for the load translational motion [14]. From (11) (when $\sigma = 1$), we can obtain

$$\boldsymbol{d}_p = m_l(\ddot{\boldsymbol{p}}_l + \boldsymbol{g}_3) - \boldsymbol{F}_t. \tag{21}$$

Let $\hat{\boldsymbol{d}}_p$ denote the estimated disturbance and $\boldsymbol{e}_p$ introduce the observer error as

$$\boldsymbol{e}_p = \boldsymbol{d}_p - \hat{\boldsymbol{d}}_p. \tag{22}$$

Then, a disturbance observer is designed as

$$\dot{\hat{\boldsymbol{d}}}_p = \boldsymbol{L}_p\boldsymbol{e}_p = -\boldsymbol{L}_p\hat{\boldsymbol{d}}_p + \boldsymbol{L}_p(m_l\ddot{\boldsymbol{p}}_l + m_l\boldsymbol{g}_3 - \boldsymbol{F}_t), \tag{23}$$

where $\boldsymbol{L}_p$ is a user-defined matrix. In (23), the acceleration $\ddot{\boldsymbol{p}}_l$ is often inaccessible in many control systems and difficult to accurately estimate from the velocity $\dot{\boldsymbol{p}}_l$ due to measurement noise. Therefore, an auxiliary variable vector is introduced as

$$\boldsymbol{z}_p = \hat{\boldsymbol{d}}_p/m_l - \boldsymbol{L}_p\dot{\boldsymbol{p}}_l. \tag{24}$$

By calculating the time derivative of (24) and applying (23), we get

$$\dot{\boldsymbol{z}}_p = -\boldsymbol{L}_p\hat{\boldsymbol{d}}_p/m_l + \boldsymbol{L}_p(\boldsymbol{g}_3 - \boldsymbol{F}_t/m_l). \tag{25}$$

Rewrite (24), the estimated disturbance is obtained as

$$\hat{\boldsymbol{d}}_p = m_l(\boldsymbol{z}_p + \boldsymbol{L}_p\dot{\boldsymbol{p}}_l). \tag{26}$$

To prove the stability of the NDO, we obtain the time derivative of the observer error as $\dot{\boldsymbol{e}}_p = \dot{\boldsymbol{d}}_p - \dot{\hat{\boldsymbol{d}}}_p$ from (22). As we have no prior knowledge about the derivative of the real disturbance $\boldsymbol{d}_p$, we suppose the disturbance is slowly varying over time, thus $\dot{\boldsymbol{d}}_p \approx 0$. By combining (23), we have $\dot{\boldsymbol{e}}_p + \boldsymbol{L}_p\boldsymbol{e}_p = 0$. It shows that the observer is globally exponentially stable by choosing $\boldsymbol{L}_p = \text{diag}\{c_p, c_p, c_p\}$ with $c_p > 0$ [14]. More specifically, c_p specifies the exponential convergence rate.

In a similar manner, the NDOs for cable attitude and drone rotational dynamics are designed as follows

$$\dot{\boldsymbol{z}}_c = -\boldsymbol{L}_c\hat{\boldsymbol{d}}_c/(m_v l) + \boldsymbol{L}_c((\dot{\boldsymbol{q}}_c^T\dot{\boldsymbol{q}}_c)\boldsymbol{q}_c - \boldsymbol{q}_{c\times}(\boldsymbol{q}_{c\times}\boldsymbol{F}_u)/(m_v l))$$
$$\hat{\boldsymbol{d}}_c = m_v l(\boldsymbol{z}_c + \boldsymbol{L}_c\dot{\boldsymbol{q}}_c) \tag{27}$$
$$\dot{\boldsymbol{z}}_v = -\boldsymbol{L}_v\mathbf{J}_v^{-1}\hat{\boldsymbol{d}}_v + \boldsymbol{L}_v\mathbf{J}_v^{-1}(\omega_{v\times}^V\mathbf{J}_v\omega_v^V - \boldsymbol{\tau}_u)$$
$$\hat{\boldsymbol{d}}_v = \boldsymbol{z}_v + \boldsymbol{L}_v\mathbf{J}_v\boldsymbol{\omega}_v^V. \tag{28}$$

B. Control Law for Cargo Drones

We have the reference state of the slung load as $\hat{\boldsymbol{q}}_l^r = \boldsymbol{q}_c^r + \boldsymbol{p}_l^r\epsilon$ and $\hat{\boldsymbol{\xi}}_l^r = \dot{\boldsymbol{q}}_c^r + \dot{\boldsymbol{p}}_l^r\epsilon$. The reference yaw angle of the drone is given as ψ_v^r. Then we get $\hat{q}_v^r$ and twist $\hat{\xi}_v^r$ as the reference configuration of the drone. The error dynamics of dual quaternion $\hat{q}_{ve}$ and $\hat{\xi}_{ve}^V$ have been defined as

$$\hat{q}_{ve} = \hat{q}_v^{r*} \otimes \hat{q}_v, \tag{29}$$
$$\hat{\xi}_{ve}^V = \hat{\xi}_v^V - Ad_{\hat{q}_{ve}^*}\hat{\xi}_v^r. \tag{30}$$

In the above equations, $\hat{q}_v^{r*}$ is the conjugate of $\hat{q}_v^r$ and $Ad_{\hat{q}_{ve}^*}\hat{\xi}_v^r$ denotes the adjoint transformation. For details, readers can refer to our previous work [7].

By taking the derivative of $\hat{\xi}_{ve}^V$, we get

$$\dot{\hat{\xi}}_{ve}^V = \dot{\hat{\xi}}_v^V - E_{\hat{q}_{ve}^*}\hat{\xi}_v^r \tag{31}$$

with $E_{\hat{q}_{ve}^*}\hat{\xi}_v^r = \dot{\hat{q}}_{ve}^* \otimes \hat{\xi}_v^r \otimes \hat{q}_{ve} + Ad_{\hat{q}_{ve}^*}\dot{\hat{\xi}}_v^r + \hat{q}_{ve}^* \otimes \hat{\xi}_v^r \otimes \dot{\hat{q}}_{ve}$. From (15), we have

$$\dot{\hat{\xi}}_{ve}^V = \hat{F}_v + \hat{u}_v - E_{\hat{q}_{ve}^*}\hat{\xi}_v^r. \tag{32}$$

Then, a dual quaternion control law has been adopted to cancel the non-linearities of the drone subsystem $\dot{\hat{\xi}}_v^V = \hat{F}_v + \hat{u}_v$ [8], and we get

$$\hat{u}_v = -2\hat{\boldsymbol{k}}_{pv}\ln\lambda\hat{q}_{ve} - \hat{\boldsymbol{k}}_{vv}\hat{\xi}_{ve}^V - \hat{F}_v + E_{\hat{q}_{ve}^*}\hat{\xi}_v^r, \tag{33}$$

where $\hat{\boldsymbol{k}}_{pv} = \boldsymbol{k}_{pvr} + \boldsymbol{k}_{pvd}\epsilon$ and $\hat{\boldsymbol{k}}_{vv} = \boldsymbol{k}_{vvr} + \boldsymbol{k}_{vvd}\epsilon$ are control gains. Both of them are dual vector quaternions. Meanwhile, we introduce λ to tackle the two equilibria problem for dual quaternion representation. We define $\hat{q}_{ve.rw}$ as the scalar part of the rotation quaternion. Then λ is described as

$$\lambda = \begin{cases} 1 & \text{if} \quad 0 \le \hat{q}_{ve.rw} \\ -1 & \text{otherwise.} \end{cases} \tag{34}$$

Combining (4), (5) and (33), we obtain the control commands for the drone

$$\boldsymbol{\tau}_u = \mathbf{J}_v(\dot{\boldsymbol{\omega}}_v^V + \boldsymbol{a}_v) - \hat{\boldsymbol{d}}_v \tag{35}$$
$$\boldsymbol{F}_u^V = m_v(\ddot{\boldsymbol{p}}_v^V + \boldsymbol{g}_3^V) + \sigma\boldsymbol{F}_t^V + sm_v(\boldsymbol{F}_{vd} + \boldsymbol{g}_3^V). \tag{36}$$

$\boldsymbol{F}_{vd}$ is the vector of the dual part of (19). The control command angular acceleration $\dot{\boldsymbol{\omega}}_v^V$ and linear acceleration $\ddot{\boldsymbol{p}}_v$ of the drone are obtained from (33) as

$$\dot{\boldsymbol{\omega}}_v^V = -\boldsymbol{k}_{pvr}\overline{\boldsymbol{\theta}}_{ve} - \boldsymbol{k}_{vvr}\boldsymbol{\omega}_{ve}^V \tag{37}$$
$$\ddot{\boldsymbol{p}}_v^V = (-\boldsymbol{k}_{pvd}\boldsymbol{p}_{ve} - \boldsymbol{k}_{vvd}\dot{\boldsymbol{p}}_{ve})^V, \tag{38}$$

where $\overline{\boldsymbol{\theta}}_{ve}$ is the rotation angle error by natural logarithm mapping of quaternion $\bar{q}_{ve}$. $\bar{q}_{ve}$ is obtained by substituting the reference attitude $\bar{q}_v^r$ (41) (when the drone is underactuated) into (29). $\boldsymbol{\omega}_{ve}^V$ is drone's body rate error.

Considering that a quadrotor, used in this work, is an under-actuated system, the actual force exerted by the motors is given by

$$\boldsymbol{F}_u^V = [0\ 0\ ||\boldsymbol{F}_u^V||]^T = [0\ 0\ 1]^T||\boldsymbol{F}_u^V|| = \boldsymbol{b}||\boldsymbol{F}_u^V||. \tag{39}$$

For the attitude of the quadrotor, a quaternion $\bar{q}_t$ exists that rotates the quadrotor such that the thrust force vector $\boldsymbol{F}_u^V$ coincides with the desired control force $\boldsymbol{F}_u$ in the inertial frame, and it is defined using (40) [18].

$$\bar{q}_t = \frac{[\boldsymbol{b}^T\boldsymbol{F}_u + ||\boldsymbol{F}_u||, \boldsymbol{b}_\times\boldsymbol{F}_u]}{|||[\boldsymbol{b}^T\boldsymbol{F}_u + ||\boldsymbol{F}_u||, \boldsymbol{b}_\times\boldsymbol{F}_u]|||}. \tag{40}$$

The above equation ensures that $\bar{q}_t$ is a unit quaternion. The given reference rotation quaternion $\bar{q}_{zr}$ is able to be calculate from ψ_v^r, then the final reference attitude of the drone $\bar{q}_r$ is completed using a quaternion product [18]

$$\bar{q}_v^r = \bar{q}_{zr} \otimes \bar{q}_t. \tag{41}$$

From (35) and (36), when $\sigma = 0, s = 1$, it is a NDO-based dual quaternion controller for the drone [8]. Now we discuss the situation when $\sigma = 1$ and the dynamics of the drone and slung load are coupled.

Using the dual vector quaternion error dynamics of the slung load, we define the tracking errors as

$$\hat{\boldsymbol{q}}_{le} = \boldsymbol{q}_{ce} + \boldsymbol{p}_{le}\epsilon \tag{42}$$

$$\hat{\boldsymbol{\xi}}_{le} = \dot{\boldsymbol{q}}_{ce} + \dot{\boldsymbol{p}}_{le}\epsilon. \tag{43}$$

For the error terms, we have $\boldsymbol{p}_{le}$ and $\dot{\boldsymbol{p}}_{le}$ are the load position and velocity errors as

$$\boldsymbol{p}_{le} = \boldsymbol{p}_l - \boldsymbol{p}_l^r \tag{44}$$

$$\dot{\boldsymbol{p}}_{le} = \dot{\boldsymbol{p}}_l - \dot{\boldsymbol{p}}_l^r. \tag{45}$$

The slung load attitude errors are defined by $\boldsymbol{q}_{ce}$ and $\dot{\boldsymbol{q}}_{ce}$ as

$$\boldsymbol{q}_{ce} = \boldsymbol{q}_{c\times}\boldsymbol{q}_{c\times}\boldsymbol{q}_c^r \tag{46}$$

$$\dot{\boldsymbol{q}}_{ce} = \dot{\boldsymbol{q}}_c - \boldsymbol{q}_{c\times}^r\dot{\boldsymbol{q}}_{c\times}^r\boldsymbol{q}_c. \tag{47}$$

Here, we define $\boldsymbol{q}_c^d$ to indicate the calculated desired attitude of the slung load, which is determined by the position error, the velocity error, and the reference acceleration $\ddot{\boldsymbol{p}}_l^r$.

$$\boldsymbol{q}_c^d = \frac{\boldsymbol{k}_{pld}\boldsymbol{p}_{le} + \boldsymbol{k}_{vld}\dot{\boldsymbol{p}}_{le} - \mathcal{F}}{||\boldsymbol{k}_{pld}\boldsymbol{p}_{le} + \boldsymbol{k}_{vld}\dot{\boldsymbol{p}}_{le} - \mathcal{F}||}, \tag{48}$$

with $\mathcal{F} = (m_v + m_l)(\ddot{\boldsymbol{p}}_l^r + \boldsymbol{g}_3) + m_v l(\dot{\boldsymbol{q}}_c^T\dot{\boldsymbol{q}}_c)\boldsymbol{q}_c$.

To handle the slack cable condition, we design a strategy as

$$\boldsymbol{q}_c^r = \sigma\boldsymbol{q}_c^d + s\boldsymbol{q}_c^u, \tag{49}$$

where we have $\boldsymbol{q}_c^u$ as a user-defined direction vector to proceed with the drone control based on the current states of the slung load, which is set as $[0, 0, -1]$ during *Setup* and *Landing* (in Sec. V). $\boldsymbol{q}_c^r$ will be used as the reference desired load attitude in (46). Accordingly, we replace $\ddot{\boldsymbol{p}}_v^V$ in (7) using

$$\ddot{\boldsymbol{p}}_v^V = s\ddot{\boldsymbol{p}}_v^V + \sigma(\ddot{\boldsymbol{p}}_l - l\ddot{\boldsymbol{q}}_c)^V \tag{50}$$

This can be explained as: when the cable is slack with $s = 1$, there is no tension on the cable; so the load is in free fall, and the drone is a separate rigid body. Once the load is under control again where the cable is taut with $\sigma = 1$, the dynamics of the load and drone are coupled.

Then by substituting (50), (10), and (12) into (36), we are able to calculate the control force as

$$\boldsymbol{F}_u = m\ddot{\boldsymbol{p}}_l - \boldsymbol{d}_p m/m_l - m_v l\ddot{\boldsymbol{q}}_c + \boldsymbol{d}_c + m\boldsymbol{g}_3, \tag{51}$$

with $m = m_v + m_l$. We can see $m\ddot{\boldsymbol{p}}_l$ is the component for the load position control and $-m_v l\ddot{\boldsymbol{q}}_c$ is the item for the slung load attitude control. The position and attitude controllers are designed respectively as

$$\ddot{\boldsymbol{p}}_l = -\boldsymbol{k}_{pld}\boldsymbol{p}_{le} - \boldsymbol{k}_{vld}\dot{\boldsymbol{p}}_{le} + \ddot{\boldsymbol{p}}_l^r \tag{52}$$

$$\ddot{\boldsymbol{q}}_c = -\boldsymbol{k}_{plr}\boldsymbol{q}_{ce} - \boldsymbol{k}_{vlr}\dot{\boldsymbol{q}}_{ce}, \tag{53}$$

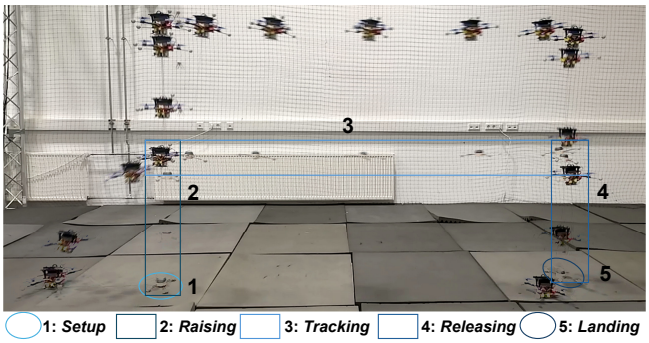

Fig. 3: The cargo drone's load transportation mission is divided into several phases: *Setup*: The load remains on the ground while the drone hovers above it. *Raising*: The drone lifts the load to the desired height. *Tracking*: The drone transports the load along a predefined trajectory. *Releasing*: The load is released at the target location. *Landing*: The drone lands next to the released load.

with $\hat{k}_{pl}$, and $\hat{k}_{vl}$, $\boldsymbol{k}_{cp}$ as control gains. Since the cable cannot transmit torque due to its physical properties, the direction of the tension is along the cable, and we obtain

$$\boldsymbol{F}_u = m(\boldsymbol{q}_c^T\ddot{\boldsymbol{p}}_l\boldsymbol{q}_c - \boldsymbol{d}_p/m_l) - m_v l\ddot{\boldsymbol{q}}_c + \boldsymbol{d}_c + m\boldsymbol{g}_3 \tag{54}$$

Then we replace (36) using $\boldsymbol{F}_u^V = \bar{q}_v^* \otimes \boldsymbol{F}_u \otimes \bar{q}_v$.

TABLE I: Parameters of the Cargo Drone System

Cargo Drone	$m_v = 0.817\,\text{kg}$, $m_l = 0.225\,\text{kg}$, $l = 0.86\,\text{m}$
Trajectory	$r = 1.2\,\text{m}$, $H = 0.8\,\text{m}$, $\omega_l^r = 0.4\pi/s$, $\boldsymbol{p}_l^r = [r * \sin(\omega_l^r * t), r * \cos(\omega_l^r * t), H]$, $\psi_v^r = \arctan(\dot{p}_{ly}^r/\dot{p}_{lx}^r)$
Geo. Gains	$\hat{\boldsymbol{k}}_{pv} = [0, 9, 9, 15, 0, 8, 8, 10.0]$ $\hat{\boldsymbol{k}}_{vv} = [0, 2.0, 2.0, 2.0, 0, 5.5, 5.5, 5.5]$ $\hat{\boldsymbol{k}}_{pl} = [0, 40, 40, 30, 0, 7.2, 7.2, 8]$ $\hat{\boldsymbol{k}}_{vl} = [0, 8.0, 8.0, 8.0, 0, 3.2, 3.2, 3.2]$
DQ. Gains	$\hat{\boldsymbol{k}}_{pv} = \hat{\boldsymbol{k}}_{pv}$, $\hat{\boldsymbol{k}}_{vv} = \hat{\boldsymbol{k}}_{vv}$ $\hat{\boldsymbol{k}}_{pl} = [0, 30, 30, 20, 0, 3.5, 3.5, 5.5]$ $\hat{\boldsymbol{k}}_{vl} = [0, 7.5, 7.5, 7.5, 0, 3.2, 3.2, 3.2]$

V. Cargo Transportation Using Drones

To verify the NDO-based dual quaternion control strategy proposed in this work, we conducted full cargo transportation missions, consisting of five steps/modes [19] as shown in Fig. 3:

Setup (Set.): The load is initially placed on the ground at a safe distance with the drone. During the *Setup* period, the drone has to fly to the point above the load from the initial position, where we have $s = 1$. The drone's reference position is determined by (49) and (9) with $\boldsymbol{q}_c^u = [0, 0, -1]$.

Raising (Rai.): After *Setup* mode, the cargo drone will start *Raising* mode with $\sigma = 1$. The load is expected to reach a desired height, which is given by H in Table I.

Tracking (Tra.): The load is tracking a predefined trajectory to finish the transportation mission with $\sigma = 1$.

Releasing (Rel.): The load reaches the target point. The drone needs to release the load on the ground with $\sigma = 1$.

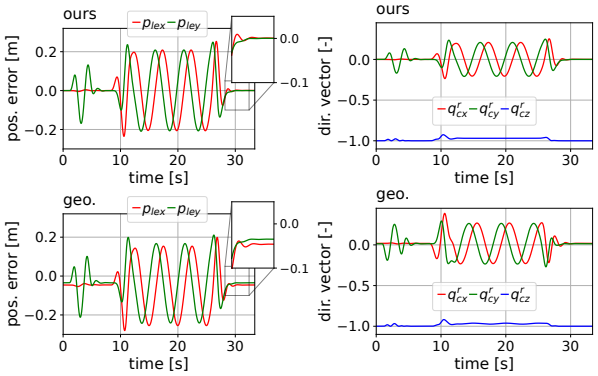

Fig. 4: The plots depict the comparison results of tracking error when the offset vector is not zero.

TABLE II: Numerical Verification Results

	Trajectories with different angular velocities ω_l^r [rad s^{-1}]						
RMSE[m]	0.2π	0.3π	0.4π	0.5π	0.6π	0.7π	0.8π
ours	0.016	0.021	0.035	0.059	0.121	0.229	failed
geo.	0.017	0.021	0.038	0.063	failed	failed	failed

Landing (Lan.): During this phase, the drone lands next to the load with $s = 1$.

We implemented our proposed control strategy and the geometric controller [3] in simulation under various conditions. The controller's performance is evaluated by comparing position tracking errors on circular reference trajectories with a radius of r at a height of H, as detailed in Table I. The angular velocity of the trajectory ω_l^r ranges from 0.2π rad s^{-1} to 0.7π rad s^{-1}. The proposed control strategy is assessed through numerical simulations using a time step of 0.01 s.

1) With Ideal Model: We first conducted simulations to track predefined trajectories using ideal models, as described in Sec. III. In these simulations, we assume complete knowledge of the cargo drone system, including the drone and slung load mass, inertia, cable length, and the attachment point being precisely located at the drone's CoM. These ideal-model experiments demonstrate the best possible performance each controller can achieve. The system parameters are shown in Table I.

Tracking performances across various circular trajectory frequencies are summarized in Table II. At low frequencies, the tracking error difference between our NDO-based dual quaternion control strategy and the geometric controller is minimal, with both achieving root mean square errors (RMSE) of less than 0.1 m during the tracking mission. This result is expected, as the simulation parameters perfectly match the dynamic model. As the trajectory frequency increases, the geometric controller becomes unstable and ultimately fails to complete the simulation.. In contrast, our NDO-based dual quaternion control strategy successfully completes the tracking task, although with an increase in tracking error, where the observer we designed enhances the robustness of the controller.

In both simulations, only first-order feedforward terms are implemented. While incorporating higher-order feedforward terms is theoretically possible, they often fail to enhance performance in practice due to increased sensitivity to model mismatches and discretization noise. Even in a simulated environment, the system is subject to residual unmodeled effects, such as numerical integration errors and latent actuator dynamics, which are not explicitly captured in the control law.

Our proposed method leverages NDOs to compensate for these residual effects in real-time. By treating these unmodeled dynamics as external disturbances, the NDO provides an adaptive feedback correction that significantly enhances robustness and safety—particularly during high-speed maneuvers and highly dynamic transitions.

2) With Mismatches of the Model: To evaluate the robustness of the proposed strategy, we introduced a model mismatch in the form of a non-zero offset $\boldsymbol{r} = [0.06, 0.06, -0.03]^\top$m between the load attachment point and the drone's CoM. The resulting performance is illustrated in Fig. 4. As shown in the tracking error plots (left), the proposed controller significantly reduces steady-state errors compared to the baseline geometric controller. This improvement is further evidenced by the reference cable direction vector $\boldsymbol{q}_c^r$ (right). In the presence of the CoM offset, the geometric controller converges to a biased $\boldsymbol{q}_c^r \neq [0, 0, -1]^\top$ to compensate for the unmodeled moment. In contrast, our NDO-based strategy effectively estimates and rejects this disturbance, allowing $\boldsymbol{q}_c^r$ to recover to the nominal vertical position $[0, 0, -1]^\top$ within an absolute tolerance of 0.002. Furthermore, the plots of $\boldsymbol{q}_c^r$ also indicate that the proposed method effectively damps load oscillations, thereby enhancing system stability under mismatched conditions. These results validate that the integrated NDO successfully compensates for parametric uncertainties, ensuring high-fidelity load tracking for the cargo drone system.

VI. Experimental Results

The real-world experiments are designed to validate the performance of our proposed control strategy. Readers can refer to the supplementary video provided in the Appendix to get a clearer understanding of the stability and effectiveness of our method.

All experiments were conducted on the Agilicious drone platform [20], where the state estimation, communication, and control pipeline run in real-time on the drone using a Jetson onboard computer. The control commands are computed in the form of desired collective thrust and body rates, and are tracked by a low-level PID controller, so the NDO for the drone rotational dynamics is only used in simulation. A user interface on a ground station (Fig. 2) enables sending mission commands such as take-off, transportation, and release of the load.

A. Experiment 1: Cargo Transportation

In this experiment, the cargo drone successfully executed a full-load transportation mission. To evaluate the controller's performance, the angular velocity of the reference circular trajectory was dynamically varied from 0.2π rad s^{-1} to 0.5π rad s^{-1}. Hardware experiments inherently involve various uncertainties and disturbances. These include imprecise knowledge of the cable length due to its flexibility and slight

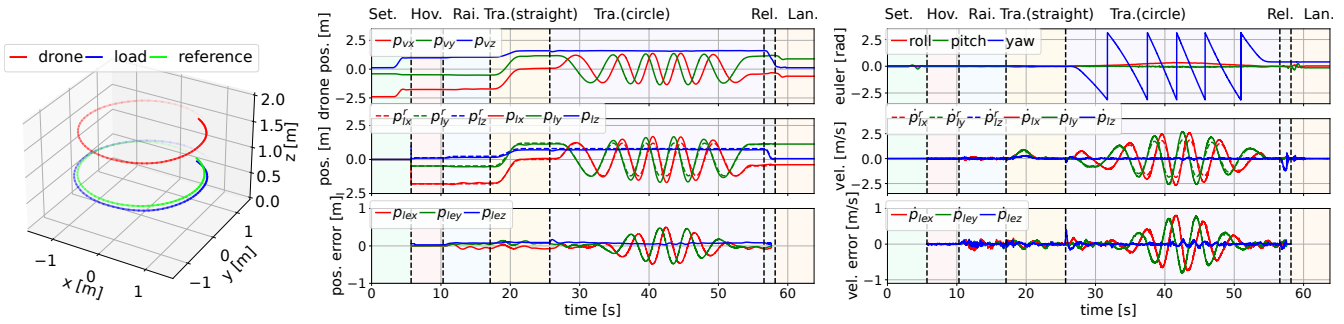

(a) The 3D trajectories. (b) The positions of the drone and the load. (c) The drone's euler angle and the load's velocity.

Fig. 5: Exp. 1: The load transportation mission with a time-varying circular trajectory. The left figure depicts the 3D trajectories. The middle plot shows the position and tracking error during the mission. The right plot shows the Euler angles of the drone (from $\bar{q}_v$) and the velocity of the load. The red line is the x direction, the green line is the y direction, and the blue line is the z direction.

elasticity, aerodynamic asymmetries of the drone body, and misalignment between the cable attachment point and the drone's center of mass. Additionally, environmental factors such as wind and unmodeled aerodynamic effects further complicate the control problem. Despite these challenges, our control strategy demonstrates strong robustness. The integrated NDOs effectively compensate for these uncertainties and disturbances in real-time.

The experimental results are presented in Fig. 5. Fig. 5(a) shows the 3D trajectories of the drone, the load, and the load's reference. The result plot indicates that the load closely tracks the reference trajectory, validating the practical performance of our approach. Figure 5(b) provides a detailed breakdown of the mission phases. The top panel displays the drone's position, while the middle and bottom panels show the load's trajectory tracking and the corresponding error residuals. The data indicates that the system achieves rapid stabilization during the takeoff phase, maintaining a steady-state tracking error of less than 0.05 m. During the *Setup* phase, the drone establishes a stable hover directly above the payload. Upon transitioning to the *Raising* mode, the cable direction vector $\boldsymbol{q}_c$ remains approximately aligned with the gravity direction $[0, 0, -1]^\top$. This alignment, evidenced by the minimal deviation between the drone and load positions, confirms that the load swing was successfully suppressed during vertical displacement.

The dynamic response is further analyzed in Fig. 5(c). The Euler angles (top panel) show that the drone's attitude adjusts fluidly to provide the necessary centripetal force as the load's velocity increases. Notably, the second and third plots in Fig. 5(c) demonstrate that the load's velocity tracks the time-varying reference. Upon completion of the mission, the velocities rapidly converge to near-zero values. This rapid attenuation of kinetic energy underscores the controller's ability to minimize residual oscillations, ensuring a safe and precise delivery.

B. Experiment 2: Robustness Test

To assess the robustness of the proposed control strategy, we conducted a series of experiments in which the cargo drone system was subjected to external disturbances. Specifically, we attached a horizontal rope either to the drone (i) or to the load (ii). The rope was connected via a pulley to a freely hanging weight with a mass of $30\,\mathrm{g}$. Once released, this setup generated a constant horizontal force disturbance of approximately $0.294\,\mathrm{N}$.

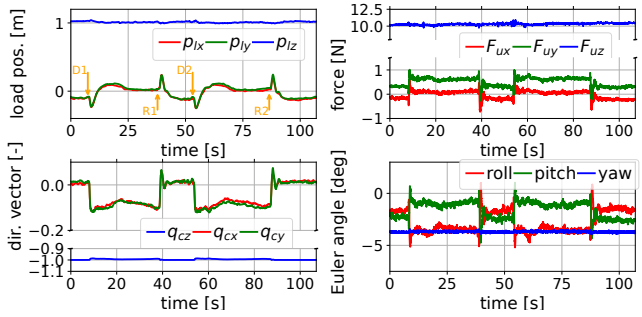

Fig. 6: Exp.2: Two identical force disturbances are applied to the load, as shown in the top-left plot. D_n indicates the moment when the disturbance is applied, and R_n marks its release. The effect of these disturbances is analyzed on the load position $\boldsymbol{p}_l$, the cable attitude vector $\boldsymbol{q}_c$, the control force $\boldsymbol{F}_u$, and the drone's attitude represented in Euler angles.

Disturbance on the slung load: In the first test, we applied a series of two force disturbances directly to the load, displacing it from its initial position. As shown in the top-left subfigure of Fig. 6, the onset of each disturbance is marked by D_n, while the release is indicated by R_n. The displacement of the load is clearly visible; however, the controller promptly compensates for the disturbance, exhibiting only a small overshoot. The remaining subfigures illustrate the system's response: the top-right subfigure shows the control force, the bottom-left depicts the direction vector of the cable, and the bottom-right presents the drone's attitude (Euler angles). Upon each disturbance, the controller rapidly stabilizes the load, with the compensation settling within approximately $5\,\mathrm{s}$. This rapid recovery demonstrates the effectiveness of our control approach in suppressing load oscillations and maintaining system stability under external perturbations. Such performance is essential for real-world

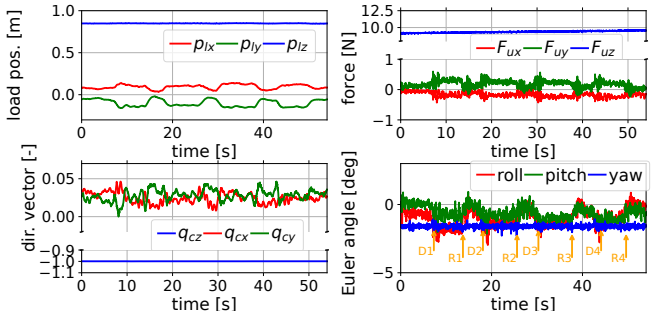

Fig. 7: Exp. 2: Four identical force disturbances are applied to the drone, as shown in the lower-right plot. D_n indicates the moment when each disturbance is applied, and R_n marks its release. The effects of these disturbances are observed on the load position $\boldsymbol{p}_l$, the cable attitude vector $\boldsymbol{q}_c$, the control force $\boldsymbol{F}_u$, and the drone's attitude represented in Euler angles.

applications, particularly in challenging environments with wind gusts or when the load undergoes sudden shifts during transport.

Disturbance on the drone: In the second test, we applied a series of four force disturbances directly to the drone body. The corresponding results are shown in Fig. 7. The drone immediately compensates for each disturbance by adjusting its attitude (lower-right plot). The perturbations in the load position and load direction vector (plots on the left side) remain marginal, with a maximum position change of less than $[2, 6, 0.5]$ cm.

These experiments demonstrate the robustness of our control strategy against disturbances acting on both the load and the drone. The combination of dual quaternion-based modeling and NDO enables the system to swiftly dampen oscillations and restore stability, thereby ensuring safe and precise transportation operations under real-world uncertainties.

VII. Conclusion

This paper proposes a hybrid dual quaternion-based control strategy that incorporates NDOs to rapidly estimate and compensate for external disturbances, thereby improving system stability and robustness. The simulation and hardware experimental results confirm the practical effectiveness of the approach, especially at higher speeds (angular velocity exceeds 0.6π rad s^{-1}) and under uncertainties and disturbances. The real high-speed flight test achieves tracking errors under 0.4 m and demonstrates rapid disturbance rejection with minimal oscillations.

Despite these promising results, several important research directions remain for future work. A critical next step is to develop and validate reliable onboard state estimation methods for slung-load position and velocity that do not rely on external motion capture systems such as VICON. Meanwhile, we expect to apply the proposed unified dual quaternion framework to multiple drones with a shared cable-suspended load to achieve load full-pose control. Furthermore, we will improve the control strategy to enable more efficient and higher-speed transportation missions. Additionally, integrating real-time obstacle avoidance mechanisms will be essential for practical deployment in complex environments. Addressing these challenges will contribute to making drone-based cargo transportation more reliable and adaptable to real-world conditions.

References

[1] G. Macrina, L. D. P. Pugliese, F. Guerriero, and G. Laporte, "Drone-aided routing: A literature review," *Transportation Research Part C: Emerging Technologies*, vol. 120, p. 102762, 2020.

[2] H. M. Omar, R. Akram, S. M. Mukras, and A. A. Mahvouz, "Recent advances and challenges in controlling quadrotors with suspended loads," *Alexandria Engineering Journal*, vol. 63, pp. 253–270, 2023.

[3] K. Sreenath, T. Lee, and V. Kumar, "Geometric control and differential flatness of a quadrotor uav with a cable-suspended load," in *52nd IEEE Conference on Decision and Control*. IEEE, 2013, pp. 2269–2274.

[4] M. Sarvaiya, G. Li, and G. Loianno, "HPA-MPC: Hybrid Perception-Aware Nonlinear Model Predictive Control for Quadrotors with Suspended Loads," *IEEE Robotics and Automation Letters*, vol. 10, pp. 358–365, 1 2025.

[5] J. Kang and J. Shan, "Virtual Nonholonomic Constraints-Based Motion Control for Underactuated UAV Slung-Payload Systems," *IEEE Transactions on Automatic Control*, vol. 70, no. 10, pp. 7047–7054, 10 2025.

[6] S. Li, T. T. Duong, and D. Zanotto, "In-Flight Cable Length Control for Improved Quadrotor-Based Suspended Load Transportation," *IEEE Robotics and Automation Letters*, vol. 9, no. 1, pp. 667–674, 1 2024.

[7] Y. Yuan and M. Ryll, "Dual Quaternion Control of UAVs with Cable-suspended Load," in *2024 IEEE International Conference on Robotics and Automation (ICRA)*. IEEE, 5 2024, pp. 1561–1567.

[8] X. Wang and C. Yu, "Unit dual quaternion-based feedback linearization tracking problem for attitude and position dynamics," *Systems & Control Letters*, vol. 62, no. 3, pp. 225–233, 2013.

[9] J. Kang and J. Shan, "Trajectory Planning for UAV Transportation Systems Using RRT*-Informed NMPC," in *2024 IEEE International Conference on Systems, Man, and Cybernetics (SMC)*. IEEE, 10 2024, pp. 994–998.

[10] M. Steinberger, I. Castillo, M. Horn, and L. Fridman, "Robust output tracking of constrained perturbed linear systems via model predictive sliding mode control," *International Journal of Robust and Nonlinear Control*, vol. 30, no. 3, pp. 1258–1274, 2 2020.

[11] H. Wang, H. Li, B. Zhou, F. Gao, and S. Shen, "Impact-Aware Planning and Control for Aerial Robots With Suspended Payloads," *IEEE Transactions on Robotics*, vol. 40, pp. 2478–2497, 2024.

[12] J. Wang and M. Krstic, "Output-Positive Adaptive Control of Hyperbolic PDE-ODE Cascades," 9 2023.

[13] J. Kang and J. Shan, "Coupling-Enhanced Smooth Adaptive Control for Underactuated UAV-Slung-Payload Systems," *IEEE/ASME Transactions on Mechatronics*, vol. 30, no. 6, pp. 7066–7076, 12 2025.

[14] W. H. Chen, D. J. Ballance, P. J. Gawthrop, and J. O'Reilly, "A nonlinear disturbance observer for robotic manipulators," *IEEE Transactions on Industrial Electronics*, vol. 47, no. 4, pp. 932–938, 2000.

[15] A. Moeini, A. F. Lynch, and Q. Zhao, "Disturbance observer-based nonlinear control of a quadrotor UAV," *Advanced Control for Applications: Engineering and Industrial Systems*, vol. 2, no. 1, p. e24, 3 2020.

[16] N. Dantam, "Quaternion computation," *Georgia Institute of Technology, Atlanta, Tech. Rep*, 2014.

[17] T. Lee, M. Leok, and N. H. McClamroch, "Geometric tracking control of a quadrotor uav on se (3)," in *49th IEEE conference on decision and control (CDC)*. IEEE, 2010, pp. 5420–5425.

[18] H. Abaunza, P. Castillo, A. Victorino, and R. Lozano, "Dual quaternion modeling and control of a quad-rotor aerial manipulator," *Journal of Intelligent & Robotic Systems*, vol. 88, pp. 267–283, 2017.

[19] P. J. Cruz and R. Fierro, "Cable-suspended load lifting by a quadrotor uav: hybrid model, trajectory generation, and control," *Autonomous Robots*, vol. 41, pp. 1629–1643, 2017.

[20] P. Foehn, E. Kaufmann, A. Romero, R. Penicka, S. Sun, L. Bauersfeld, T. Laengle, G. Cioffi, Y. Song, A. Loquercio, and D. Scaramuzza, "Agilicious: Open-source and open-hardware agile quadrotor for vision-based flight," *Science Robotics*, vol. 7, no. 67, 5 2022.